OPEN ACCESS
Journal of Innovative Optical Health Sciences
Vol. 15, No. 6 (2022) 2250035 (13 pages)

DOI: 10.1142/S1793545822500353

Ultrasmall pH-responsive silicon phthalocyanine micelle for selective photodynamic therapy against tumor

Yiming Zhou*,||, Wenlong Zeng*,||, Mengxuan Wang*,||, Rui Li*,
Xiuli Yue†,‡,¶ and Zhifei Dai*,§,¶
*Department of Biomedical Engineering, College of Future Technology
Peking University, Beijing 100871, P. R. China
†School of Environment, Harbin Institute of Technology
Harbin 150001, P. R. China
‡xiulidx@163.com
§zhifei.dai@pku.edu.cn

Received 20 April 2022
Accepted 29 June 2022
Published 27 September 2022

Targeted photodynamic therapy (TPDT) based on the photosensitizers responsive for tumor microenvironment is promising because of the better anti-tumor effect and less phototoxicity against normal tissue than the traditional PDT. Nanoparticle-based stimuli-responsive photosensitizers have been widely explored for TPDT. Based on the acidic microenvironments in solid tumors, an ultrasmall pH-responsive silicon phthalocyanine nanomicelle (PSN) (smaller than 10 nm) was designed for selective PDT of tumor. PSN had high drug loading efficacy (more than 28%) and exhibited morphological transitions, enhanced fluorescence and improved singlet oxygen yield under acidic environments. PSN was renal clearable and could rapidly accumulate and be retained at tumor sites, achieving a tumor-inhibiting effect better than phthalocyanine micelle without pH response. Tumors of mice treated with PSN for PDT were completely ablated without recurrence. Thus, we have developed a phthalocyanine-based pH-responsive micelle with excellent tumor targeting ability, which is expected to realize the selective PDT of tumor.

Keywords: Silicon phthalocyanine; pH-responsive; ultrasmall micelle; targeted photodynamic therapy.

1. Introduction

In order to further enhance the effect of tumor photodynamic therapy (PDT) and reduce the damage to normal tissues, targeted PDT has been proposed through designing photosensitizers that aim at tumor characteristics.[1–5] Compared with inefficient passive targeting dominated by the enhanced permeability and retention (EPR) effect, the active targeting strategies based on tumor-specific molecular recognition have attracted more and

¶Corresponding authors.
||Yiming Zhou, Wenlong Zeng, and Mengxuan Wang contributed equally to this work.

more attention. In view of excellent antigen specificity, monoclonal antibodies have become the first choice for tumor targets.[6,7] ASP-1929, a photosensitizer drug composed of cetuximab and water-soluble silicon phthalocyanine, is already in clinical trials.[8,9] In addition, other target molecules such as peptides,[10–13] folic acid[14–17] as well as glycosyl[18,19] have also been tried, accompanied by good tumor enrichment and retention. However, the damage of these actively targeted photosensitizers to normal tissues is inevitable on account of their high photosensitivity during blood circulation.

Ideal photosensitizers should maintain low or even no photosensitivity in the blood circulation but be specifically activated at the tumor site. This activatable strategy is considered to be an effective method for solving the deficient selectivity of photosensitizers.[20–25] The tumor microenvironment (TME) exhibits many unique properties such as faintly acidic pH, high expression of matrix metalloproteinase and glutathione, which provides excellent response sites for triggered PDT against tumor.[26–29] Moreover, high reactive oxygen species (ROS) produced during PDT were also utilized to restore photosensitizer activity at the tumor site.[30,31] Among them, the universality of acidic TME regardless of the tumor types or the developmental stages enables the pH-activatable photosensitizer with extreme potential.

The large amount of lactic acid resulted from the unique glycolysis of tumor cells that transforms TME into a faintly acidic state in sharp contrast with normal weakly alkaline physiological environments. This acidic microenvironment exists in almost all solid tumors, making pH response an attractive broad-spectrum tumor target for selective PDT.[32–36] Some pH-sensitive units such as amino groups and amino acids have been used to construct pH-activated phthalocyanines with good pH response and anti-tumor effects.[37,38] Nevertheless, poor water solubility forces these phthalocyanine molecules to require vast excipients for aiding injection. Coupling with polymers or silica to form nanoparticles is conducive to improving the solubility of phthalocyanine, while it also introduces some new defects, including low drug loading capacity, complex synthesis, difficult degradation and metabolism, and potential biotoxicity.[39–45]

To address the aforementioned limitations, we designed an ultrasmall pH-responsive silicon phthalocyanine nanomicelle (PSN) by attaching amino groups and polyethylene glycol (PEG) on two sides of the silicon phthalocyanine axis, respectively. Covalent bonding enables PSN to possess a high drug loading capacity and prevent the phthalocyanine from leaking during blood circulation. Inherent amphiphilicity promotes PSN to self-assemble into micelles beneficial to drug injection and delivery so that PSN locates tumors through the EPR effect. The photon-induced electron transfer (PET) effect of amino groups will keep PSN low in fluorescence and photosensitivity during blood circulation to minimize the toxicity to normal tissues. Once PSN reaches tumor sites, acidic TME

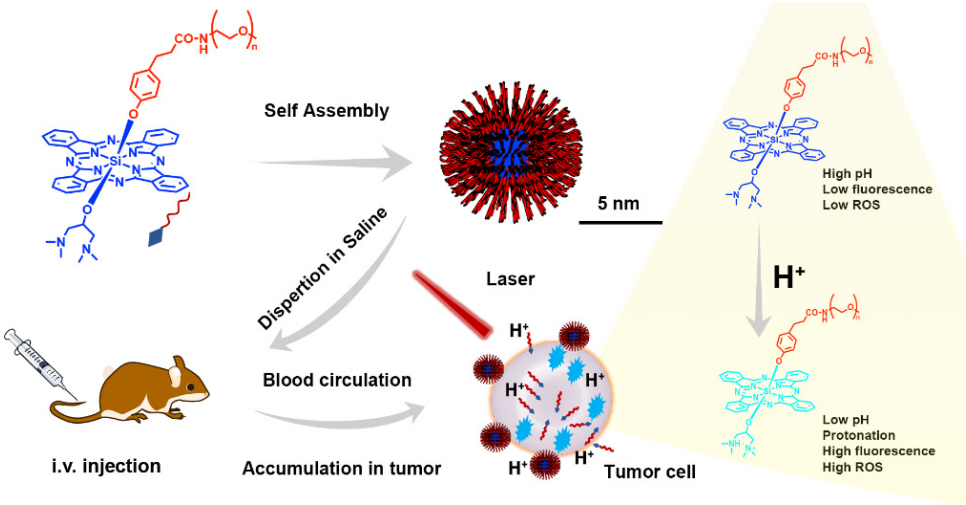

Scheme 1. Schematic illustration of pH-responsive ultrasmall silicon phthalocyanine micelles for selective photodynamic therapy against tumor.

protonates amino groups to reduce the PET effect, thereby restoring the fluorescence and photodynamic activity of PSN. Furthermore, positive charges after protonation can promote the uptake and retention of PSN by tumor cells, which further enhances the photodynamic anti-tumor effect of PSN (Scheme 1). Thus, PSN is a pH-responsive photosensitizer that can specifically kill tumors with negligible damage to normal tissues, and it has broad application prospects for selective PDT against tumor.

2. Experimental Section

2.1. *Materials*

1,3-diiminoisoindoline and p-hydroxyhydrocinnamic acid were purchased from Tianjin Heowns Biochemical Technology Co., Ltd. Silicon tetrachloride was obtained from Beijing Innochem Technology Co., Ltd. 1,3-Bis(dimethylamino)-2-propanol was acquired from Sigma-Aldrich. Aminopolyethylene glycol 2000 was purchased from Hefei Bomei Biochemical Technology Co., Ltd. 1-ethyl-3-(3-dimethylaminopropyl) carbodiimide (EDC) was gained from Shanghai Aladdin Bio-Chem Technology Co., Ltd. 1,3-diphenylisobenzofuran (DPBF) was purchased from Ark Pharm, Inc. DCFH-DA was obtained from Jiangsu KeyGEN BioTECH Co., Ltd. CCK-8 cell viability assay kit was purchased from Shanghai Beyotime Biotechnology Co., Ltd. Lysotracker was acquired from Suzhou Meilun Biotechnology Co., Ltd. 4′,6-diamidino-2-phenylindole (DAPI) and Apoptosis Detection Kit were gained from Beijing Solarbio Science & Technology Co., Ltd. Dulbecco's modified Eagle medium (DMEM) and Fetal Bovine Serum (FBS) were purchased from Thermo Fisher Scientific. Other reagents were of analytical grade and were employed without further purification.

2.2. *Synthesis of PSN (Fig. S1)*

2.2.1. *Synthesis of silicon phthalocyanine dichloride*

The solution of 1,3-diiminoisoindoline (10 g) and silicon tetrachloride (10 mL) in quinoline (200 mL) was heated to 180°C for 2 h. After cooling to room temperature, it was poured into 400 mL dimethyl formamide (DMF) followed by suction filtration. The filter residue was repeatedly washed with chloroform, dichloromethane, methanol, acetone, tetrahydrofuran, and benzene until the filtrate was colorless. A pure bright purple solid was obtained as silicon phthalocyanine dichloride (11.2%) after drying.

2.2.2. *Synthesis of PEG-p-hydroxyphenylpropionic acid intermediate*

p-Hydroxyphenylpropionic acid (83 mg) and EDC (105 mg) in anhydrous DMF (5 mL) were stirred for 10 min at ambient temperature. Then, PEG-NH_2 (100 mg) was added and the mixture was stirred overnight. The crude product after removing solvent was purified with a silica gel column (eluent: methanol:dichloromethane = 1:15, 1% glacial acetic acid was added) to obtain the PEG-p-hydroxyphenylpropionic acid intermediate (82.5%).

2.2.3. *Synthesis of compound* 1

Silicon phthalocyanine dichloride (100 mg), sodium hydride (16.4 mg) and 1,3-bis(dimethylamino)-2-propanol (95 mg) in anhydrous toluene (15 ml) were refluxed for 24 h. The crude product, after removing solvent, was purified via a basic alumina column with ethanol/chloroform (1:9) as the eluent. ^{1}H NMR (500 MHz, $CDCl_3$) δ 9.61 (dd, $J = 5.5, 3.0$ Hz, 8H), 8.29 (dd, $J = 5.7$, 2.8 Hz, 8H), 0.48 (s, 24H), −0.80 (dd, $J = 12.5$, 5.4 Hz, 4H), −1.56 (dd, $J = 12.4$, 5.1 Hz, 4H), −2.64 to −2.79 (m, 2H) (Fig. S3).

2.2.4. *Synthesis of PSN (compound* 2*)*

Compound 1 (100 mg), sodium hydride (4.8 mg) and PEG-p-hydroxyphenylpropionic acid intermediate (240 mg) in toluene (15 ml) were refluxed overnight. The crude product, after removing solvent, was purified via a basic alumina column with triethylamine/ethyl acetate (1:1000) as the eluent. PSN (23.8%) was obtained by collecting blue-green bands. ^{1}H NMR (500 MHz, $CDCl_3$) δ 9.62 (s, 8H), 8.34 (s, 8H), 3.71–3.52 (m, 175H), 2.34–1.98 (m, 11H), 1.71 (dd, $J = 18.4$, 10.4 Hz, 4H), 0.52 (s, 3H), 0.48 (s, 8H), −0.75 (s, 1H), −1.55 (s, 1H), −2.50 to −2.77 (m, 1H) (Fig. S5).

2.3. *Preparation of PSN micelles*

The solution of PSN in DMF (100 μL) with a concentration of 10 mg/mL was dropped into

phosphate buffer solution (PBS) solution (2 mL) with the aid of water bath ultrasound. Then, the mixed solution was concentrated via ultrafiltration, accompanied by DMF removal. The phthalocyanine concentration was determined through the standard curve for subsequent experiments.

2.4. *Transmission electron microscope (TEM) characterization*

A small amount of PSN suspension at different pHs was added onto a copper mesh (carbon supported film, 30 mesh) and absorbed for 10 min, followed by being negatively stained with 1% phosphotungstic acid for 10 min. After natural drying at room temperature, the sample was exposed to TEM with an accelerating voltage of 100 kV, to record its size and morphology.

2.5. *Singlet oxygen yield test in aqueous solutions with different pH*

Ethanol solution of DPBF and an aqueous solution of PSN at pH 6.5 or 7.4 were mixed in a cuvette. Then, the mixed solution was irradiated by laser for certain durations, and the absorption spectra were recorded to obtain changes in absorbance at 414 nm with the ultraviolet spectrophotometer. The absorbance before illumination was regarded as the initial value A_0, and this value was changed to A_t after different irradiation times. The curve that reflected singlet oxygen yield was plotted by taking time as the horizontal axis and $\ln(A_0/A_t)$ as the vertical axis. The larger slope of the curve represented the higher singlet oxygen yield.

2.6. *Cell culture and cellular uptake experiment*

4T1 murine breast cancer cells were cultured in DMEM including 10% FBS and 1% penicillin/streptomycin. In order to study cellular uptake, 4T1 cells were seeded on a 96-well plate at the density of 1×10^4 per well and cultured overnight. The preseeded cells were then incubated with 1 μM PSN for different times, followed by a fluorescence microscope to observe and capture intracellular fluorescence and the software ImageJ for quantitative analysis.

Then, the subcellular localization of PSN was investigated. 4T1 cells were seeded on 35 mm dishes at the density of 2×10^4 per dish and cultured overnight. Then, the preseeded cells were incubated with 1 μM PSN for 4 h and washed with PBS thrice. After being stained with Lysotracker for 30 min and washed again, cells were fixed with 70% ethanol for 10 min, followed by DAPI treatment for 15 min and three-time PBS washing. Afterward, co-localization images were obtained with a confocal laser scanning microscopy (Nikon A1R high-speed confocal laser microscope, Nikon Corporation, Japan). By analyzing an arbitrary straight line crossing a certain cell in the picture using ImageJ, the spatial change was plotted to further quantify the co-localization of lysosome and PSN.

2.7. *In vitro photocytotoxicity evaluation*

To detect intracellular ROS, 4T1 cells were seeded on a 96-well plate at the density of 1×10^4 per well and cultured overnight. The preseeded cells were then incubated with 1 μM PSN for 4 h, followed by incubation with 10 μM DCFH-DA for 30 min. Then, the cells were replaced with fresh DMEM and exposed to a xenon lamp for certain periods of time. The production of intracellular ROS was qualitatively and quantitatively analyzed with a fluorescence microscope and a microplate reader, respectively.

Then, the cells were seeded in the same way to study the photosensitivity of PSN. After incubation with PSN at different concentrations for 4 h, the cells were replaced with fresh DMEM and subjected to dark treatment or laser irradiation treatment, followed by incubation with CCK-8 for 1 h. Then, absorbance at 450 nm was measured by a microplate reader to calculate cell viability. To further realize the mechanism of cell death, 4T1 cells were seeded on a 6-well plate at the density of 5×10^5 per well and cultured overnight. Then, the preseeded cells were incubated with 200 nM PSN for 4 h and replaced with fresh DMEM, followed by dark treatment or laser irradiation treatment. The apoptosis and necrosis rate of cells were measured using an apoptosis detection kit through the flow cytometer.

2.8. *In vivo fluorescence imaging*

Female Balb/c mice aged 6–8 weeks were purchased from BeijingVital River Laboratory Animal Technology Co., Ltd. All animal experiments were

approved by the Peking University Institutional Animal Care and Use Committee (IACUC). An orthotopic breast cancer model was established by injecting 2×10^7 4T1-luci tumor cells into the fourth pair of mammary glands of each mouse. The volumes of tumors reached approximately $100\,\text{mm}^3$ about 6 days after injection and were used for fluorescence imaging *in vivo*. Then, PSN dissolved in PBS (pH = 7.4) was intravenously injected into the orthotopic tumor-bearing mice with a dose of $1\,\mu$mol/kg. At different time points after the injection, a living animal fluorescence imaging system was used for fluorescence imaging with excitation at 660 nm, and the fluorescence signal was collected using a 700 nm filter. The data were analyzed by the FOBI software to get accumulation process of PSN at tumors.

2.9. *In vivo photodynamic therapy*

PDT was performed 7 days after the establishment of the orthotopic breast tumor model, and the average initial tumor volume was $100\,\text{mm}^3$. The mice were randomly divided into four groups ($n = 5$): Group 1 with PBS, Group 2 with PSN, Group 3 with PM + light and Group 4 with PSN + light. First, PSN ($2\,\mu$mol/kg), PM ($2\,\mu$mol/kg) and PBS, each of $200\,\mu$L were intravenously injected to the corresponding groups. Tumor areas of Groups 3 and 4 were irradiated 4 h later using a 671 nm laser ($0.2\,\text{W/cm}^2$) for 16 min with a total laser intensity of $192\,\text{J/cm}^2$. After treatment, the tumor size was measured for each mouse every day using the electronic vernier calipers for 15 days. The maximum width (X) and length (Y) of each tumor were measured, and the following formula was used to calculate the tumor volume: $V = (X^2Y)/2$. The weight changes of each group were also recorded each day. Tumors in each group were randomly selected to be excised for H&E, TUNEL and Ki67 assay to analyze the tumor apoptosis, proliferation and necrosis. In order to investigate the biological safety of PDT with PSN, major organs (heart, liver, spleen, lung and kidney) of each group were also dissected for H&E staining to evaluate the pathological changes after the treatment.

2.10. *Statistical analysis*

Data were presented as mean ± standard deviation (SD). Student's t-test was employed to test the significance of the difference, which was considered to be significant when $^*P < 0.05$.

3. Results and Discussion

3.1. *Synthesis of PSN*

A simple two-step synthesis method was used to synthesize asymmetric PSN in this paper (Fig. S1). Phthalocyanine silicon dichloride was synthesized by the reaction of isoindole and silicon tetrachloride in quinolone, followed by purification with precipitation and organic solvent washing. Then, phthalocyanine silicon dichloride and 1,3-bis (dimethylamino)-2-propanol underwent bilateral axial substitution reaction to obtain compound 1. After purification by basic alumina column chromatography, a unilateral nucleophilic reaction between compound 1 and PEG polymer with phenol active groups produced a PEG-phthalocyanine conjugate with pH response as the final product (compound 2, PSN). It is worth noting that the ratio of compound 1 and PEG polymer must be strictly controlled to minimize the formation of a by-product with bilateral nucleophilic substitution. PSN was purified with basic alumina column chromatography for subsequent experiments.

3.2. *In vitro pH responsiveness of PSN*

pH responsiveness is the key to reducing the phototoxicity of PSN to normal tissues. Various methods were used to investigate the responsive capacities of PSN to pH changes. Under a weakly alkaline condition (pH = 7.4), the inherent amphiphilic property promoted PSN to self-assemble into uniform micelles with mean diameters of less than 10 nm, which has been confirmed by the TEM image and dynamic light scattering measurement. Whereas, when the solution became faintly acidic (pH = 6.5), protonation of dimethylamino turned PSN into hydrophilic molecules, thus resulting in the disintegration of micelles (Figs. 1(a) and S7). In order to observe the pH response characteristics of PSN more visually, PSN dissolved in solutions with two inverse pH were imaged by a small animal live imager. As shown in Fig. 1(b), the fluorescence intensity of PSN in a faintly acidic PBS is twice that of a weakly alkaline PBS. A more precise measurement was carried out via fluorescence spectroscopy, and the results displayed that faintly acidic

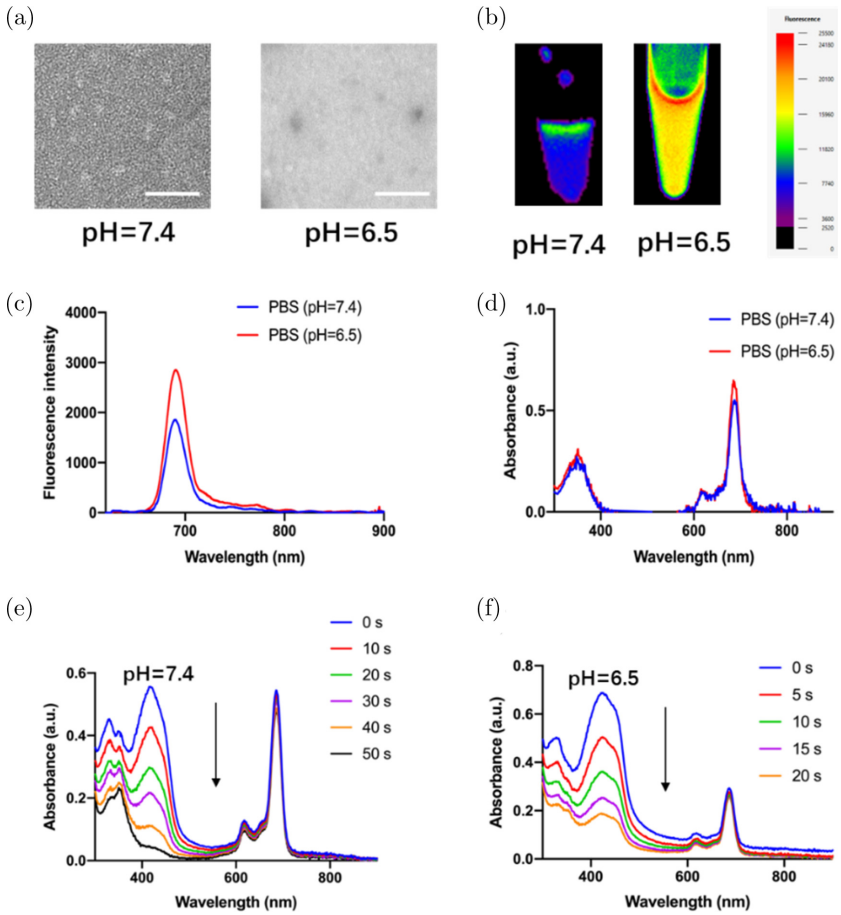

Fig. 1. Responsive capacities of PSN micelles to pH changes in PBS (pH = 7.4 and pH = 6.5). (a) Representative TEM micrographs (scale bar: 50 nm). (b) Fluorescence imaging results excited by 660 nm. (c) Fluorescence emission spectra excited by 610 nm. (d) UV–Vis absorption spectra of PSN. UV–Vis absorption spectra of PSN and DPBF in PBS with pH = 7.4 (e) and pH = 6.5 (f) after light irradiation for different time.

conditions increased the fluorescence intensity by half [Fig. 1(c)]. This enhancement might be attributed to weakening of the PET effect after protonation rather than molecular disaggregation. The absorption spectrum also supported this inference because the absorption spectra of PSN in different pH PBS both presented a typical monomer state with a sharp absorption peak in the Q band [Fig. 1(d)], implying the dispersed state of PSN molecules in the micelles.

Compared with fluorescence, the ability to generate singlet oxygen is the crucial indicator for measuring the photodynamic killing effects of photosensitizers. It is necessary to investigate the effect of pH changes on the singlet oxygen yield of PSN. Singlet oxygen can oxidize DPBF with a characteristic absorption peak at 414 nm into DBB without absorption, so absorption spectra that measured changes in absorbance at 414 nm were performed to estimate the generation of singlet oxygen. As shown in Figs. 1(e) and 1(f), the photobleaching rate of PSN to DBPF was slow in the pH 7.4 PBS, but it was accelerated under faintly acidic conditions. The slope of the PSN singlet oxygen yield curve under faintly acidic conditions was 1.35 times that under weakly alkaline conditions (Fig. S9), indicating the pH-responsive singlet oxygen generation capability of PSN.

3.3. *Cellular uptake and subcellular localization of PSN*

Prior to evaluating the photodynamic effects of PSN *in vitro*, it is essential to investigate cellular uptake of PSN so that the optimal laser irradiation time can be determined. After incubating 4T1 cells with PSN for 2 h, the red fluorescence of PSN was observed inside the cells by a fluorescence

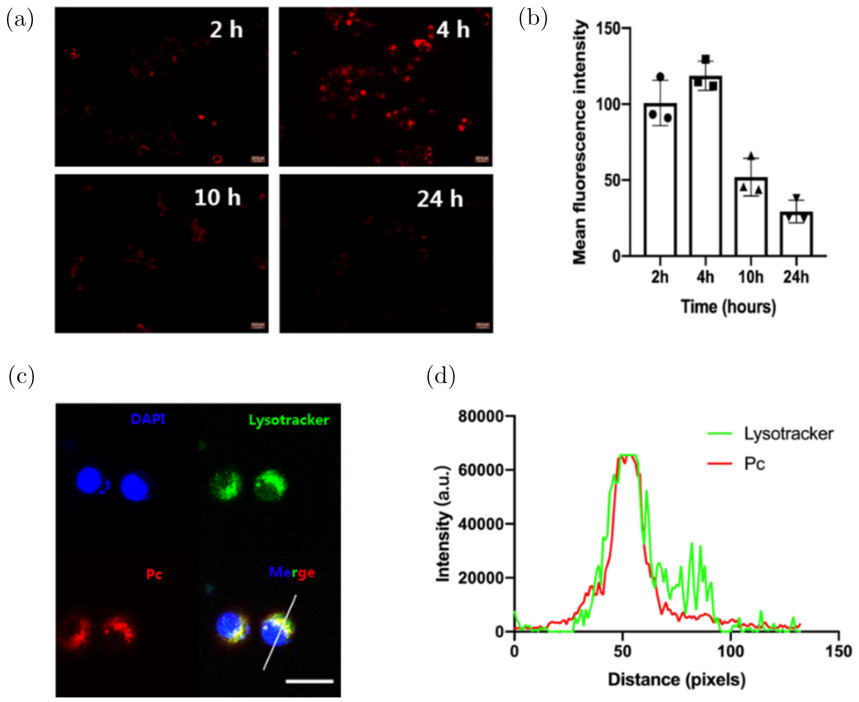

Fig. 2. Cellular internalization and subcellular localization of PSN. (a) Intracellular fluorescence changes after incubation with PSN for different time (scale bar: 20 μm). (b) Quantitative analysis of (a). (c) Confocal laser scanning microscopy images for intracellular distribution of PSN (red for PSN, green for lysosome and blue for nucleus, scale bar: 25 μm). (d) Fluorescence intensity change analysis of lysosome and phthalocyanine at the straight line in (c).

microscope. When the incubation time was extended to 4 h, the intracellular fluorescence intensities reached the highest, which implied the maximum uptake of PSN by cells [Figs. 2(a) and 2(b)]. Hence, performing laser irradiation after incubation of PSN with tumor cells for 4 h might be the optimal time for PDT *in vitro*. With the further extension of incubation time, the intracellular fluorescence gradually decreased until it almost disappeared at 24 h. However, the positive charge after protonation endowed PSN with strong cell affinity followed by longer cell retention, so cells still maintained strong fluorescence after 10 h of incubation.

Subcellular localization of PSN contributed to deeply realizing its intracellular behaviors. After incubation of PSN with 4T1 cells for 4 h, confocal imaging was performed to observe the subcellular distribution of PSN. Lysotracker with green fluorescence and DAPI with blue fluorescence were selected to mark lysosomes and nucleus, respectively. As shown in Fig. 2(c), the red fluorescence of PSN co-localized with Lysotracker instead of DAPI, manifesting the concentrated distribution of PSN in lysosomes after the uptake into the cells. The plot profile analysis of a single cell through ImageJ also supported this conclusion [Fig. 2(d)]. These results indicated that PSN could be effectively taken up by tumor cells and accumulate in acidic lysosomes to restore its fluorescence.

3.4. *pH-responsive phototoxicity of PSN against tumor cells*

The ability of PSN to produce distinct intracellular singlet oxygen under different pH conditions is one of the keys to verify the pH-responsive phototoxicity of PSN against tumor cells. In order to simulate diverse environments of tumor cells and normal cells *in vivo*, cells were cultured in media with different pH (pH = 6.5 and pH = 7.4) *in vitro*. Afterward, PSN dissolved in different pH media was incubated with cells for 4 h, succeeded by laser irradiation to generate singlet oxygen. DCFH-DA, a small molecule probe with free passage through the cell membrane, was employed for the detection of singlet oxygen. Singlet oxygen can oxidize nonfluorescent DCFH-DA into DCF with strong green fluorescence, allowing for qualitative and quantitative analysis of singlet oxygen production with

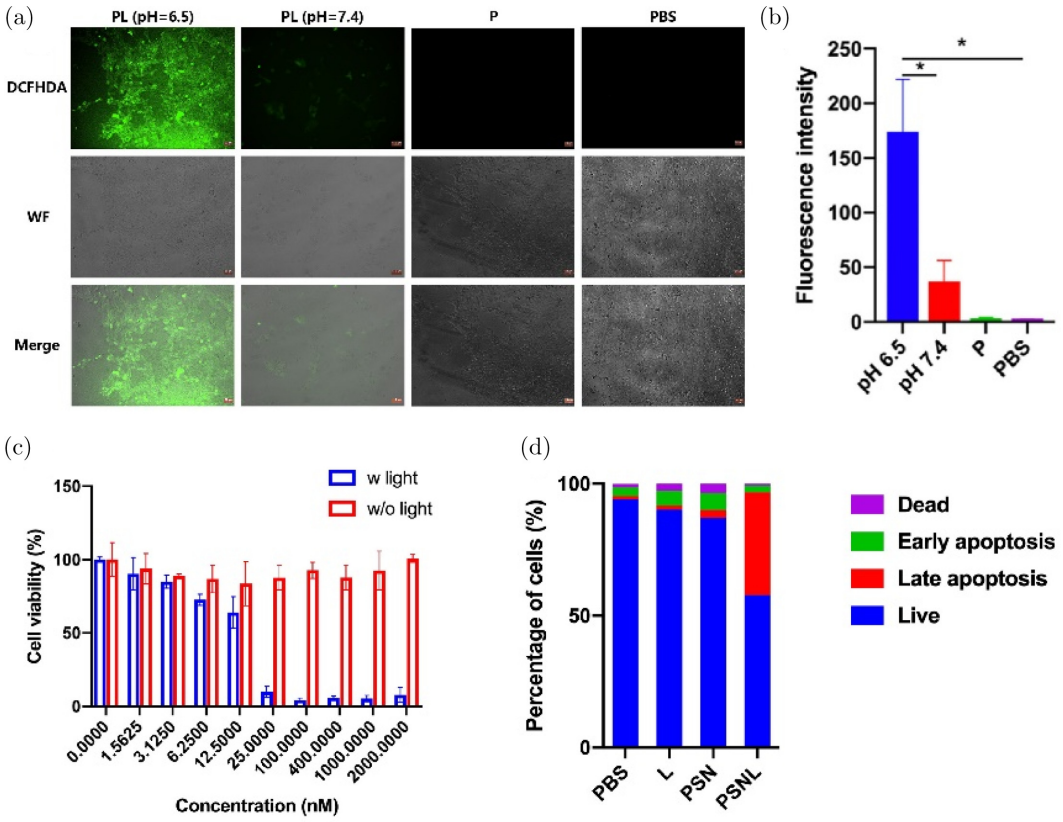

Fig. 3. pH-responsive phototoxicity of PSN against tumor cells. (a) Fluorescence images of cells incubation with PSN and DCFH-DA under different pH conditions (scale bar: 20 μm, PL for cells incubation with PSN + light, P for cells incubation with PSN only). (b) Quantitative analysis of intracellular singlet oxygen production after different treatments ($n = 3$, $^*P < 0.05$). (c) Cell viability of 4T1 cells treated by various concentration of PSN with (blue) or without (red) laser irradiation (610 nm, 48 J/cm^2, $n = 5$). (d) Quantitative analysis of cell apoptosis and necrosis after different PDT treatments through flow cytometry (L for light only, PSN for PSN only, PSNL for PSN + light).

fluorescence microscope and microplate reader. As shown in Fig. 3(a), PSN-incubated cell groups did not produce green fluorescence in the absence of laser irradiation, which was consistent with negative control groups incubated with PBS. Nevertheless, when exposed to laser irradiation, cell groups incubated with PSN under different pH conditions both exhibited green fluorescence, marking the generation of singlet oxygen. In particular, the intracellular fluorescence resulted from incubation at pH 6.5 was much stronger than that at pH 7.4, and further fluorescence quantitative analysis of DCF revealed that this amplification reached nearly fivefold [Fig. 3(b)], attesting that the acidic environment could stimulate PSN to produce a mass of intracellular singlet oxygen. These results fully declared the pH targeting properties of PSN, which meant that the photodynamic killing effect of PSN on tumor cells under acidic microenvironments was much stronger than that of normal cells even if the latter slightly took in PSN.

Based on the excellent pH responsiveness and singlet oxygen generation ability mentioned above, the cytotoxicity and photodynamic activity of PSN were evaluated by CCK-8 assay to provide safe and effective dose references for subsequent experiments. After incubating with PSN at different concentrations for 4 h, cells were subjected to dark treatment or laser irradiation treatment. As shown in Fig. 3(c), when no laser irradiation was applied, PSN had no significant impact on cell viability even though its concentration was as high as 2 μM, stating splendid safety and biocompatibility of PSN. However, under the motivation of light irradiation, PSN at a concentration of 25 nM reduced the cell survival rate to less than 15%, and a concentration of 100 nM or above killed almost all the cells. Such outstanding photodynamic activity of

PSN might be ascribed to two aspects. On the one hand, the positive charge caused by protonation of pH-responsive groups promoted the uptake of PSN by cells. On the other hand, the nonaggregated state as a result of axial modifications together with the reduction of the PET effect between PSN molecules under an acidic environment both enhanced the singlet oxygen yield of PSN. To further realize the damage mechanism of PSN to the cells, flow cytometry was utilized to analyze cell status after PDT. As shown in Fig. 3(d), the apoptotic rate of cells after PDT was as high as 38.9%, suggesting that the cell death is dominated by cell apoptosis induced by singlet oxygen.

3.5. *Tumor-specific accumulation of PSN*

Through monitoring tumor-bearing mice with a living animal fluorescence imaging system, the enrichment of PSN in tumor sites and its pH sensitivity in living animals were investigated as a prerequisite for the subsequent PDT *in vivo*. As shown in Figs. 4(a) and 4(b), tumor sites produced strong fluorescent signals 5 min after intravenous injection of PSN micelles dissolved in PBS. As time went by, fluorescence signals of tumor sites continued to increase until they reached peak values at 3 h after injection, hinting at 3 h as the best candidate for light irradiation time of PDT *in vivo*. Whereafter, tumor tissues maintained strong fluorescent signals up to 60% of the peak signals within 72 h after injection. The rapid appearance and long-term retention of fluorescent signals at tumor sites were roughly attributed to three points. First, PSN micelles could hold their nanostructures when circulating in a weakly alkaline blood physiological environment, allowing for their fast accumulation and penetration into tumor tissues through the EPR effect. Once entering tumor sites, protonation of PSN caused by the acidic TME produced strong fluorescence in tumor tissues to realize a high signal ratio to surrounding normal tissues. Lastly, positive charges after protonation enabled PSN to be easily taken in by tumor cells and retained for a long time.

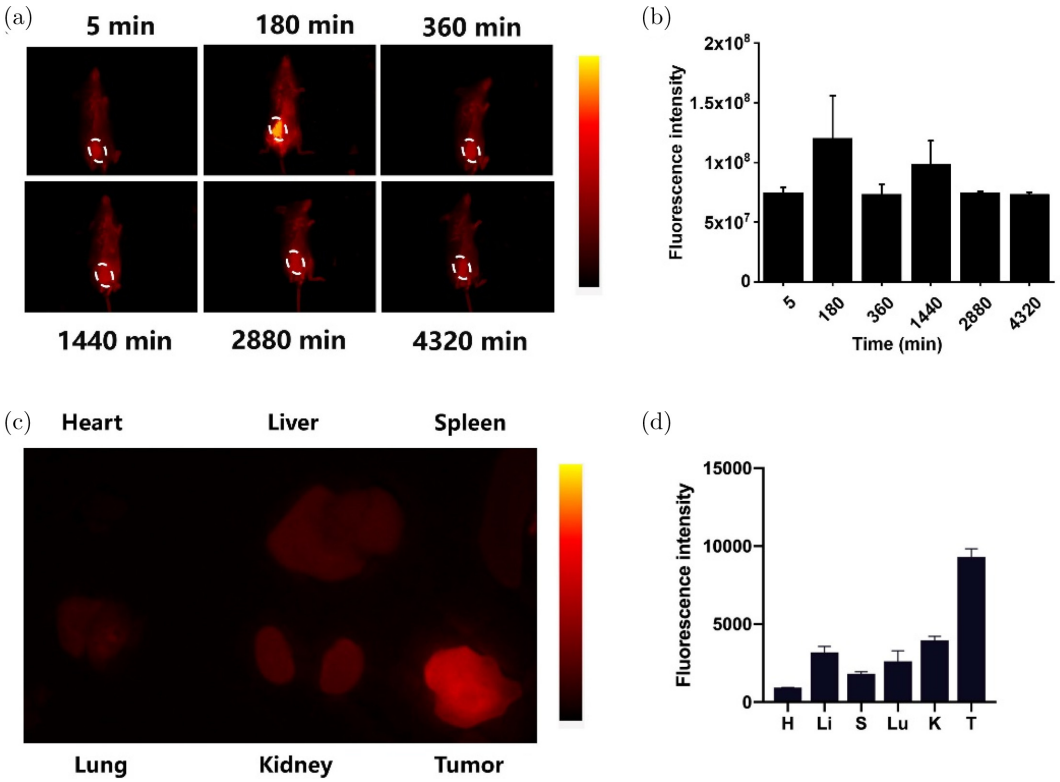

Fig. 4. *In vivo* fluorescence imaging of 4T1 tumor-bearing mice. (a) Fluorescence images of mice at different time points after intravenous injection of PSN. The dashed circles present orthotopic tumor regions. (b) Quantitative analysis of fluorescence signals at tumor sites in (a). (c) *Ex vivo* fluorescence images of major organs and tumors 24 h after intravenous injection of PSN. (d) Fluorescence quantitative analysis of (c) (H for heart, Li for liver, S for spleen, Lu for lung, K for kidney and T for tumor).

Imaging results of isolated organs further illustrated the tumor specificity of PSN caused by pH response. The mice were sacrificed 24 h after injections of PSN, and their major organs and tumors were dissected for fluorescence imaging. As shown in Figs. 4(c) and 4(d), tumor tissues presented strong fluorescence signals while fluorescent signals of other organs such as liver and kidney were pretty weak. These results indicated that PSN could enrich and restore photosensitivity at tumor sites through the EPR effect and pH response, thus leading to powerful photodynamic damage to tumor tissues. When it came to normal organs, PSN would maintain their nanostructures to weaken singlet oxygen generation ability so that side effects to normal tissues could be minimized.

3.6. *Selective PDT of PSN against tumor*

Based on the splendid tumor specificity of PSN, the *in vivo* PDT potential of PSN was investigated. In order to better compare and verify the PDT enhancement effect induced by the pH response of PSN, micelles composed of non-pH-responsive phthalocyanine (PM) and DSPE-PEG2000 were set up as a control group. In contrast to PSN micelles, PM micelles were physically embedded and insensitive to pH, so their differences were able to verify the influence of the embedding form and pH response. As shown in Fig. 5(a), tumors treated with PSN + light were completely ablated without recurrence 15 days after treatment, while the tumor volume of the group treated with PM + light only

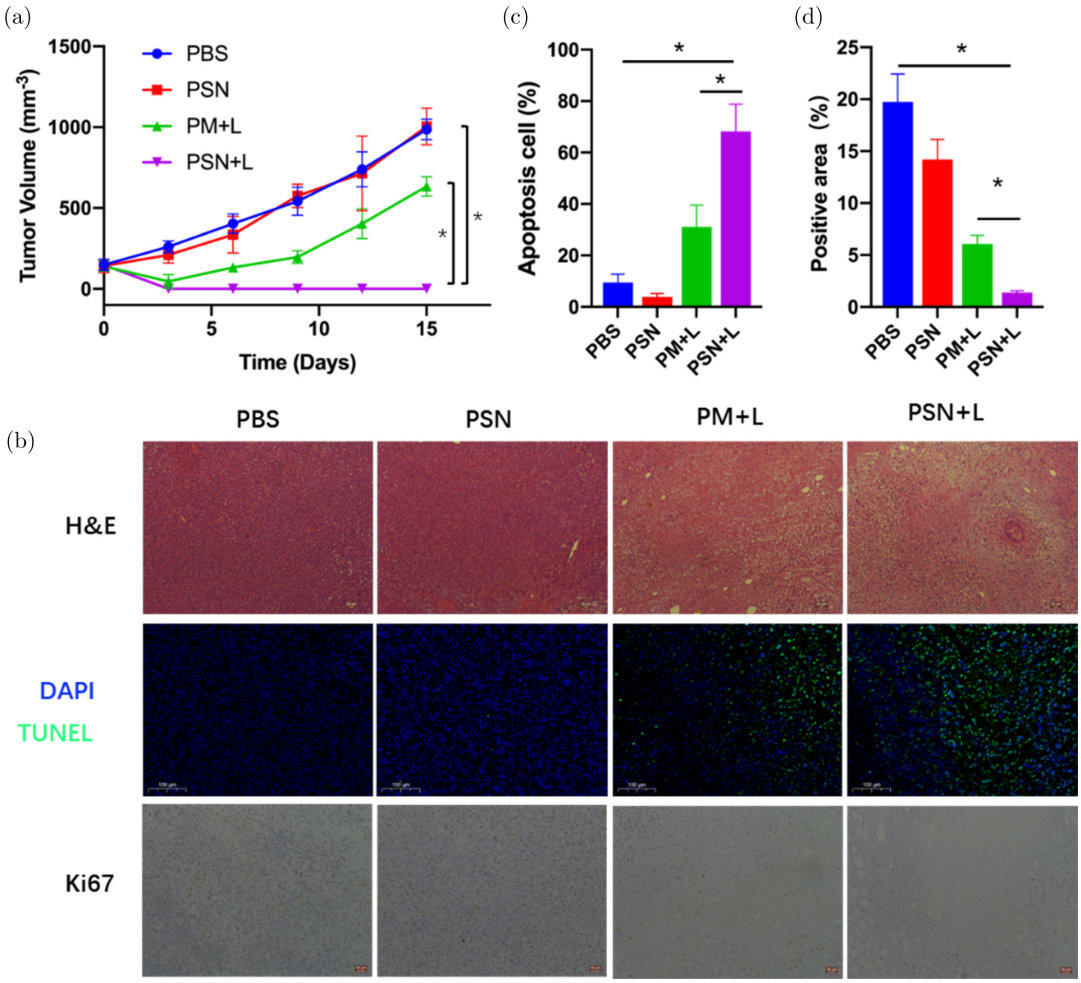

Fig. 5. *In vivo* photodynamic therapy. (a) Tumor growth curves of mice received various treatments ($n = 5$, $^*P < 0.05$). (b) Histological examination of tumors after various treatments. H&E staining images (scale bar: 20 μm), TUNEL fluorescence images (scale bar: 100 μm) and Ki67 immunohistochemical images (scale bar: 40 μm). Quantitative analysis of apoptosis cells (c) and Ki67 immunohistochemistry (d) of tumor tissue sections ($n = 3$, $^*P < 0.05$). PSN for PSN only, PM + L for PM + light and PSN + L for PSN + light.

decreased in the first 3 days of treatment but gradually increased at a rate comparable to that of the PBS-treated control group later on. Such obvious differences in therapeutic efficacy confirmed the splendid PDT potential of PSN, which might be owed to three factors. First of all, the PM + light group had a potential defect of photosensitizer leakage during blood circulation due to simple physical embedding, so its photosensitizers were less enriched at tumor sites than the PSN + light group. Next, photosensitizers in the PM + light group could not be protonated into a nonaggregated state conducive to PDT because of a lacking pH response. Third, negative charges of the carboxyl group prevented photosensitizers in the PM + light group from being effectively taken up by tumor cells.

To further reveal anti-tumor mechanisms of PSN-based PDT, tumor tissues after treatment were sliced for H&E, TUNEL and Ki67 staining [Fig. 5(b)]. As shown by TUNEL staining, no green fluorescence was observed in tumor slices of the PBS and the PSN group. In contrary, tumor slices of the PSN + light group exhibited the strongest green fluorescence, indicating the highest degree of apoptosis. Subsequent fluorescence quantitative results showed that the number of apoptosis in the PSN + light group was twice that in the PM + light group [Fig. 5(c)], so the former achieved a far better tumor suppressing effect than the latter. This apoptosis difference might be attributed to the different enrichment and cellular uptake at tumor sites as a result of disparate embedding forms and charges. Through Ki67 immunohistochemical analysis, it was observed that Ki67 staining in the PSN + light group was the least, only 1/10 of the PBS control group [Fig. 5(d)], which revealed significantly attenuated cell proliferation ability of the PSN + light group due to the strong anti-tumor effect of selective PDT. H&E staining also intuitively supported the strongest killing effect of the PSN + light group on tumors. These results all proved the superiority of pH-responsive PSN micelles for selective PDT.

Finally, the safety of PSN for PDT *in vivo* was discussed. Mouse body weight with various treatments was recorded over time. No obvious body weight change was observed among all groups (Fig. S10a), suggesting good safety of PSN-based PDT. Moreover, H&E staining pathological examination also verified that the main organs of mice treated with PSN + light were intact (Fig. S10b). Therefore, PSN is a photosensitizer with good safety, strong tumor selectivity and splendid photodynamic efficacy, which gives it a broad application prospect for selective PDT against tumor.

4. Conclusion

In summary, we have successfully designed and synthesized asymmetric PSN with pH-responsive function for selective PDT against tumors, with minimum damage to normal tissues. PSN could self-assemble into micelles under weakly alkaline conditions and exhibited feeble fluorescence and singlet oxygen generation ability on account of the PET effect. Once the environment became faintly acidic, methylamino groups of PSN were protonated, followed by disintegration of micelles together with recovery of fluorescence and singlet oxygen yield due to weakening of the PET effect. Experimental results *in vivo* declared that PSN accurately targeted tumors and retained them for a long time. Tumors of mice treated with PSN + light were completely eliminated without recurrence, which was far greater than ordinary phthalocyanine without pH response. We believe that PSN as a pH-responsive photosensitizer will have broad application prospects for selective PDT against tumor and facilitate remarkable advances in cancer therapy.

Conflict of Interest

The authors declare that there are no conflicts of interest relevant to this article.

Acknowledgments

This work was supported by grants from projects of Interdisciplinary Research Foundation of HIT, the National Natural Science Foundation of China (No. 82071980), the International Cooperation and Exchanges NSFC-PSF (No. 31961143003), the State Key Program of National Natural Science of China (No. 81930047) and the National Project for Research and Development of Major Scientifc Instruments (No. 81727803). Y. Zhou, W. Zeng and M. Wang contributed equally to this work.

References

1. A. Crous, E. Chizenga, N. Hodgkinson, H. Abrahamse, "Targeted photodynamic therapy: A novel approach to abolition of human cancer stem cells," *Int. J. Opt.* **2018**, 7317063 (2018).

2. J. C. Yan, T. Gao, Z. Z. Lu, J. B. Yin, Y. Zhang, R. J. Pei, "Aptamer-targeted photodynamic platforms for tumor therapy," *ACS Appl. Mater. Interfaces* **13**(24), 27749–27773 (2021).
3. H. H. Liu, J. W. Yao, H. H. Guo, X. W. Cai, Y. Jiang, M. Lin, X. J. Jiang, N. Leung, C. S. Xu, "Tumor microenvironment-responsive nanomaterials as targeted delivery carriers for photodynamic anticancer therapy," *Front. Chem.* **8**, 758 (2020).
4. S. Gomez, A. Tsung, Z. W. Hu, "Current targets and bioconjugation strategies in photodynamic diagnosis and therapy of cancer," *Molecules* **25**(21), 4964 (2020).
5. P. Gierlich, A. I. Mata, C. Donohoe, R. M. M. Brito, M. O. Senge, L. C. Gomes-da-Silva, "Ligand-targeted delivery of photosensitizers for cancer treatment," *Molecules* **25**(22), 5317 (2020).
6. H. Kobayashi, P. L. Choyke, "Near-infrared photoimmunotherapy of cancer," *Acc. Chem. Res.* **52**(8), 2332–2339 (2019).
7. M. Kuroki, N. Shirasu, "Novel treatment strategies for cancer and their tumor-targeting approaches using antibodies against tumor-associated antigens," *Anticancer Res.* **34**(8), 4481–4488 (2014).
8. T. Kadota, D. Kotani, Y. Yoda, M. Fukutani, M. Wakabayashi, S. Nomura, N. Fuse, A. Sato, T. Yano, K. Shitara, "A phase Ib study of near infrared photoimmunotherapy (NIR-PIT) using ASP-1929 in combination with nivolumab and for patients with advanced gastric or esophageal cancer (GE-PIT study, EPOC1901)," *J. Clin. Oncol.* **38**(4), TPS457 (2020).
9. M. A. Biel, A. M. Gillenwater, D. M. Cognetti, J. M. Johnson, A. Argiris, M. Tahara, "A global phase Ill multicenter, randomized, double arm, open label trial of ASP-1929 photoimmunotherapy versus physician's choice standard of care for the treatment of patients with locoregional, recurrent head and neck squamous cell carcinoma (rHNSCC)," *J. Clin. Oncol.* **37**(15), TPS6094 (2019).
10. E. Ranyuk, N. Cauchon, K. Klarskov, B. Guerin, J. E. van Lier, "Phthalocyanine-peptide conjugates: Receptor-targeting bifunctional agents for imaging and photodynamic therapy," *J. Med. Chem.* **56**(4), 1520–1534 (2013).
11. M. R. Ke, S. L. Yeung, W. P. Fong, D. K. P. Ng, P. C. Lo, "A phthalocyanine-peptide conjugate with high *in vitro* photodynamic activity and enhanced *in vivo* tumor-retention property," *Chem. Eur. J.* **18**(14), 4225–4233 (2012).
12. B. Y. Zheng, X. Q. Yang, Y. Zhao, Q. F. Zheng, M. R. Ke, T. Lin, R. X. Chen, K. K. K. Ho, N. Kumar, J. D. Huang, "Synthesis and photodynamic activities of integrin-targeting silicon(IV) phthalocyanine-cRGD conjugates," *Eur. J. Med. Chem.* **155**, 24–33 (2018).
13. Q. Liu, M. P. Pang, S. H. Tan, J. Wang, Q. L. Chen, K. Wang, W. J. Wu, Z. Y. Hong, "Potent peptide-conjugated silicon phthalocyanines for tumor photodynamic therapy," *J. Cancer* **9**(2), 310–320 (2018).
14. S. Wang, J. Wang, J. Y. Chen, "Conjugates of folic acids with zinc aminophthalocyanine for cancer cell targeting and photodynamic therapy by one-photon and two-photon excitations," *J. Mater. Chem. B* **2**(11), 1594–1602 (2014).
15. Y. X. Li, J. Wang, X. X. Zhang, W. J. Guo, F. Li, M. Yu, X. Q. Kong, W. J. Wu, Z. Y. Hong, "Highly water-soluble and tumor-targeted photosensitizers for photodynamic therapy," *Org. Biomol. Chem.* **13**(28), 7681–7694 (2015).
16. G. Nkepang, M. Bio, P. Rajaputra, S. G. Awuah, Y. You, "Folate receptor-mediated enhanced and specific delivery of far-red light-activatable prodrugs of combretastatin A-4 to FR-positive tumor," *Bioconjug. Chem.* **25**(12), 2175–2188 (2014).
17. Y. W. Zheng, S. F. Chen, B. Y. Zheng, M. R. Ke, J. D. Huang, "A silicon(IV) phthalocyanine-folate conjugate as an efficient photosensitizer," *Chem. Lett.* **43**(11), 1701–1703 (2014).
18. F. Lv, X. J. He, L. Wu, T. J. Liu, "Lactose substituted zinc phthalocyanine: A near infrared fluorescence imaging probe for liver cancer targeting," *Bioorg. Med. Chem. Lett.* **23**(6), 1878–1882 (2013).
19. D. Li, Q. Y. Hu, X. Z. Wang, X. S. Li, J. Q. Hu, B. Y. Zheng, M. R. Ke, J. D. Huang, "A non-aggregated silicon(IV) phthalocyanine-lactose conjugate for photodynamic therapy," *Bioorg. Med. Chem. Lett.* **30**(12), 127164 (2020).
20. X. S. Li, S. Kolemen, J. Yoon, E. U. Akkaya, "Activatable photosensitizers: Agents for selective photodynamic therapy," *Adv. Funct. Mater.* **27**(5), 1604053 (2017).
21. R. C. H. Wong, P. C. Lo, D. K. P. Ng, "Stimuli responsive phthalocyanine-based fluorescent probes and photosensitizers," *Coord. Chem. Rev.* **379**, 30–46 (2019).
22. X. S. Li, S. Yu, Y. Lee, T. Guo, N. Kwon, D. Lee, S. C. Yeom, Y. Cho, G. Kim, J. D. Huang, S. Choi, K. T. Nam, J. Yoon, "*In vivo* albumin traps photosensitizer monomers from self-assembled phthalocyanine nanovesicles: A facile and switchable theranostic approach," *J. Am. Chem. Soc.* **141**(3), 1366–1372 (2019).
23. S. Y. S. Chow, R. C. H. Wong, S. R. Zhao, P. C. Lo, D. K. P. Ng, "Disulfide-linked dendritic oligomeric phthalocyanines as glutathione-responsive photosensitizers for photodynamic therapy," *Chem. Eur. J.* **24**(22), 5779–5789 (2018).

24. M. Liu, C. H. Li, "Recent advances in activatable organic photosensitizers for specific photodynamic therapy," *ChemPlusChem* **85**(5), 948–957 (2020).
25. B. D. Zheng, J. Ye, X. Q. Zhang, N. Zhang, M. T. Xiao, "Recent advances in supramolecular activatable phthalocyanine-based photosensitizers for anti-cancer therapy," *Coord. Chem. Rev.* **447**, 214155 (2021).
26. F. Gong, N. L. Yang, X. W. Wang, Q. Zhao, Q. Chen, Z. Liu, L. Cheng, "Tumor microenvironment-responsive intelligent nanoplatforms for cancer theranostics," *Nano Today* **32**, 100851 (2020).
27. A. Jhaveri, P. Deshpande, V. Torchilin, "Stimuli-sensitive nanopreparations for combination cancer therapy," *J. Control Release* **190**, 352–370 (2014).
28. Y. H. Wu, F. N. A. Li, X. Q. Zhang, Z. Q. Li, Q. F. Zhang, W. J. Wang, D. Y. Pan, X. L. Zheng, Z. W. Gu, H. Zhang, Q. Y. Gong, K. Luo, "Tumor microenvironment-responsive PEGylated heparin-pyropheophorbide - A nanoconjugates for photodynamic therapy," *Carbohydr. Polym.* **255**, 117490 (2021).
29. N. Yang, W. Y. Xiao, X. J. Song, W. J. Wang, X. C. Dong, "Recent advances in tumor microenvironment hydrogen peroxide-responsive materials for cancer photodynamic therapy," *Nano-Micro Lett.* **12**(1), 15 (2020).
30. D. Jia, X. B. Ma, Y. Lu, X. Y. Li, S. X. Hou, Y. Gao, P. Xue, Y. J. Kang, Z. G. Xu, "ROS-responsive cyclodextrin nanoplatform for combined photodynamic therapy and chemotherapy of cancer," *Chin. Chem. Lett.* **32**(1), 162–167 (2021).
31. S. Kwon, H. Ko, D. G. You, K. Kataoka, J. H. Park, "Nanomedicines for reactive oxygen species mediated approach: An emerging paradigm for cancer treatment," *Acc. Chem. Res.* **52**(7), 1771–1782 (2019).
32. E. Boedtkjer, S. F. Pedersen, "The acidic tumor microenvironment as a driver of cancer," *Annu. Rev. Physiol.* **82**, 103–126 (2020).
33. Y. L. Dai, C. Xu, X. L. Sun, X. Y. Chen, "Nanoparticle design strategies for enhanced anticancer therapy by exploiting the tumour microenvironment," *Chem. Soc. Rev.* **46**(12), 3830–3852 (2017).
34. S. Thakkar, D. Sharma, K. Kalia, R. K. Tekade, "Tumor microenvironment targeted nanotherapeutics for cancer therapy and diagnosis: A review," *Acta Biomater.* **101**, 43–68 (2020).
35. M. Z. Jin, W. L. Jin, "The updated landscape of tumor microenvironment and drug repurposing," *Signal Transduct. Target Ther.* **5**(1), 166 (2020).
36. A. Gulzar, J. T. Xu, C. Wang, F. He, D. Yang, S. L. Gai, P. P. Yang, J. Lin, D. Y. Jin, B. G. Xing, "Tumour microenvironment responsive nanoconstructs for cancer theranostic," *Nano Today* **26**, 16–56 (2019).
37. S. F. Yan, J. C. Chen, L. Z. Cai, P. Xu, Y. X. Zhang, S. J. Li, P. Hu, X. Y. Chen, M. D. Huang, Z. Chen, "Phthalocyanine-based photosensitizer with tumor-pH-responsive properties for cancer theranostics," *J. Mater. Chem. B* **6**(38), 6080–6088 (2018).
38. A. Wang, L. Gui, S. Lu, L. Zhou, J. H. Zhou, S. H. Wei, "Tumor microenvironment-responsive charge reversal zinc phthalocyanines based on amino acids for photodynamic therapy," *Dyes Pigm.* **126**, 239–250 (2016).
39. A. R. Karimi, A. Khodadadi, M. Hadizadeh, "A nanoporous photosensitizing hydrogel based on chitosan cross-linked by zinc phthalocyanine: An injectable and pH-stimuli responsive system for effective cancer therapy," *RSC Adv.* **6**(94), 91445–91452 (2016).
40. X. H. Hu, Z. Y. Gao, H. P. Tan, L. Zhang, "A pH-responsive multifunctional nanocarrier in the application of chemo-photodynamic therapy," *J. Nanomater.* **2019**, 3898564 (2019).
41. A. L. Lin, S. Z. Li, C. H. Xu, X. S. Li, B. Y. Zheng, J. J. Gu, M. R. Ke, J. D. Huang, "A pH-responsive stellate mesoporous silica based nanophotosensitizer for *in vivo* cancer diagnosis and targeted photodynamic therapy," *Biomater. Sci. UK* **7**(1), 211–219 (2019).
42. X. S. Li, B. Y. Zheng, M. R. Ke, Y. F. Zhang, J. D. Huang, J. Yoon, "A tumor-pH-responsive supramolecular photosensitizer for activatable photodynamic therapy with minimal *in vivo* skin phototoxicity," *Theranostics* **7**(10), 2746–2756 (2017).
43. R. C. H. Wong, S. Y. S. Chow, S. Zhao, W. P. Fong, D. K. P. Ng, P. C. Lo, "pH-responsive dimeric zinc (II) phthalocyanine in mesoporous silica nanoparticles as an activatable nanophotosensitizing system for photodynamic therapy," *ACS Appl. Mater. Interfaces* **9**(28), 23487–23496 (2017).
44. X. Wang, M. H. Li, Y. H. Hou, Y. N. Li, X. M. Yao, C. C. Xue, Y. Fei, Y. Xiang, K. Y. Cai, Y. L. Zhao, Z. Luo, "Tumor-microenvironment-activated in situ self-assembly of sequentially responsive biopolymer for targeted photodynamic therapy," *Adv. Funct. Mater.* **30**(40), 2000229 (2020).
45. M. R. Song, D. Y. Li, F. Y. Nian, J. P. Xue, J. J. Chen, "Zeolitic imidazolate metal organic framework-8 as an efficient pH-controlled delivery vehicle for zinc phthalocyanine in photodynamic therapy," *J. Mater. Sci.* **53**(4), 2351–2361 (2018).